Pergamon

PII: S0191–8141(97)00101–6

Journal of Structural Geology, Vol. 20, No. 5, pp. 517 to 527, 1998

0191-8141/98 $19.00 + 0.00

Hangingwall bed rotation and the development of contractional and extensional structures around a thrust fault: geometric and experimental models

A. K. DUBEY and S. S. BHAKUNI

Wadia Institute of Himalayan Geology, Dehra Dun, 248 001, India

(*Received* 25 *April* 1997; *accepted in revised form* 15 *October* 1997)

Abstract—Tectonic inversion of normal faults, and development of extensional and contractional structures in the vicinity of thrust faults were studied using two models; (i) a geometric (or rigid) model, and (ii) an experimental (or brittle–ductile) model. The first model is based on simple trigonometric relationships between shortening, rotation of layers along a thrust, and dip of the thrust. The model may be used to understand the structures at upper levels of the Earth's crust in a predominant brittle regime. The second model is based on a series of experiments performed with clay analogues. It simulated the structures forming at a deeper level in a brittle–ductile regime and incorporates folding as an essential feature. The results of the study reveal that structures near a thrust fault depend on the thrust geometry and dip amount, the initial orientation of hangingwall layers, and their rheological properties. In the absence of frictional effects along a thrust surface, the rotation of layers and consequent displacement is directly proportional to the thrust dip. Since the listric faults are characterized by a decrease of dip with depth, the variation in the rotation of layers in a profile-section may result in formation of dilation spaces that may serve as potential sites for secondary mineral deposits or oil traps. A large rotation of hangingwall layers results in a reverse fault drag and a small rotation (caused by frictional effects along the fault) produces normal fault drag.

INTRODUCTION

The formation of rift basins involves displacement and sedimentation along a series of listric normal faults. The concave geometry of these faults (i.e. decrease of dip with depth) necessitates a rotation of the hangingwall block, resulting in layers dipping opposite to the fault (i.e. back tilting) (e.g. Ramsay and Huber, 1987, fig. 23.27). Later compression may cause inversion tectonics (Cooper and Williams, 1989), where the earlier listric normal faults are reactivated as listric thrust faults. Hangingwall layers may rotate in a reverse direction through the null point (Williams *et al*., 1989). Hence, depending on the fault type and displacement magnitude, layer dips can vary over a listric fault.

Simulated deformation of such systems has been studied by McClay and his associates in a number of publications (McClay, 1989; McClay and Ellis, 1987; McClay and Scott, 1991; Buchanan and McClay, 1991; Huiqi *et al*., 1992; McClay and Buchanan, 1992). These deformations of loose sand models demonstrate the development of listric faults, associated secondary faults and drag folds. However, the models simulated deformation in the upper 10 km of the Earth's crust (i.e. the brittle regime) where folding is unlikely to occur. Since simultaneous development of thrust faults and folds is an integral part of an orogeny, these structures should be studied in a brittle–ductile regime as well. We analysed this situation by performing experiments with modelling clay models. The present study examined thrust faults with small displacements or blind thrusts where the displacement decreased to zero at the termination. The study of thrust displacement of larger magnitudes, and detachment folds was excluded from the present study. Experimental results and variation of geometrical features were compared to a geometric model. The model involves a minimum friction along the fault and demonstrates the amount of rotation with shortening of layers for different initial orientations and fault displacement. The model is described prior to the experiments so that the geometric complexities that may arise are known.

THE GEOMETRICAL MODEL OF ROTATION OF LAYERS ALONG A PLANAR THRUST FAULT

A significant contribution regarding the geometrical relationship between fault bend folds, fault shape and cut-off angles was made by Suppe (1983), whose model is based on parallel kink band geometry of the hangingwall rocks over a decollement, and preservation of area. Another important contribution was made recently by Coward (1996), whose model describes the rotation of the fault by hangingwall folding with no fault displacement during basin inversion. We attempt to establish a relationship between fault dip and rotation of hangingwall layers during inversion, where layers rotate along the fault without any change in their length.

Figure 1 represents a fault plane A′–B with dip angle θ. A horizontal layer BC′ joins the fault at point B. A compressive stress along the layer results in rotation of the layer and displacement along the

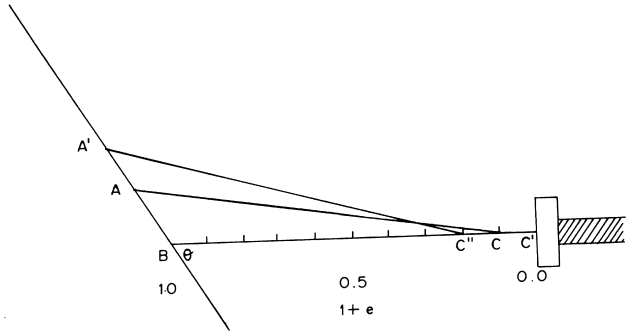

Fig. 1. A geometrical representation of rotation of a layer BC′ along a thrust fault A′B with an increase in shortening.

thrust. After a few increments of shortening, the layer occupies a new position CA, when folding is absent, layer length is unchanged, and displacement along the fault is relatively easy. The distance AB represents the fault displacement and the angle ACB represents the rotation of the layer. If the initial layer BC′ is divided into 10 equal parts then rotation of the layer can be measured for every 10% increase of shortening, e.g. the angle ACB represents a rotation after 10% shortening and the angle A′C″B represents a rotation after 20% shortening. The angle ACB (and other angles with increasing shortening) can be calculated by the following relationship

$$\cos \mathrm{ACB} = \frac{\mathrm{BC}^2 + \mathrm{AC}^2 - \mathrm{AB}^2}{2\mathrm{BC}.\mathrm{AC}}$$

With the help of the above relationship, layer dips were calculated for different fault dips with increasing shortening (Fig. 2a & b). The following inferences can be drawn from these results.

Thrust and layer dipping in the same direction

1. The dip of the layer increases steadily with shortening depending on the fault dip and initial layer dip (Fig. 2a). The rate of increase of layer dip is lower in gentle thrusts as compared to steep thrusts. Hence, a greater variation in the layer and the thrust dip leads to an initial higher increase in layer dip during shortening.
2. The individual lines on the graph (Fig. 2a) represent an orientation where the length of the layer remains constant. The region above the line represents extension whereas the region below the line represents shortening of the layer.

Thrust and layer dipping in opposite directions

1. The layer rotates clockwise with an increase in shortening thereby resulting in a decrease of dip. The rate of layer rotation is lower and nearly uniform for gently dipping layers whereas steeper layers show a greater rotation during the early stages of shortening (Fig. 2b).
2. The individual lines on the graph (Fig. 2b) represent rotation of the layer while maintaining a constant length. The region above the line (Fig. 2b) represents shortening whereas the region below the line represents stretching of the layer (cf. Fig. 2a where fault and layer dip in the same direction).
3. At fault dips of 30° and above, lines intersect prior to 10% shortening, indicating that these layers undergo early contraction (Fig. 3a). Similarly at fault dips of 60° and above, the layers shorten to rotate along the fault plane (Fig. 3b). Hence, fault dips of more than 60° could not be included in the diagram.
4. Layer dips higher than 80° were not included because; (i) layers are unlikely to be vertically oriented in a rifted terrain, and (ii) compression normal to vertical layers is likely to extend layers instead of rotation and fault displacement.
5. Layers gradually rotate to a horizontal position when additional rotation follows the pattern shown in Fig. 2.

THE EXPERIMENTAL MODEL

The experiments performed with modelling clay multilayer models simulate the simultaneous development of listric thrust faults and folds. The construction of the models and the deformation press has been described earlier (Dubey and Cobbold, 1977). A positive listric fault (i.e. steepening upward: McClay and Ellis, 1987) was cut in the models prior to deformation. The fault was confined to the multilayers and it did not penetrate into the top and bottom matrix. Layer orientation varied in different experiments as described subsequently.

Experiment 1

In this model, both the hangingwall and footwall layers were parallel to the axis of maximum shortening (Fig. 4). At the onset of deformation, thrust displacement took place along the initial fault. An asymmetric fold initiated at 7% shortening (Fig. 4b) in the hangingwall multilayers over an irregularity on the thrust surface (i.e. where the regular fault curvature was interrupted by a minor flat). Symmetric folds initiated at a horizontal distance from the thrust. Transverse fold propagation was not prominent so folds propagated upward in the multilayers and gradually modified to a box fold geometry. The symmetric and asymmetric folds amplified with occasional formation of hinge dilation (Ramsay, 1974). The fold amplifica-

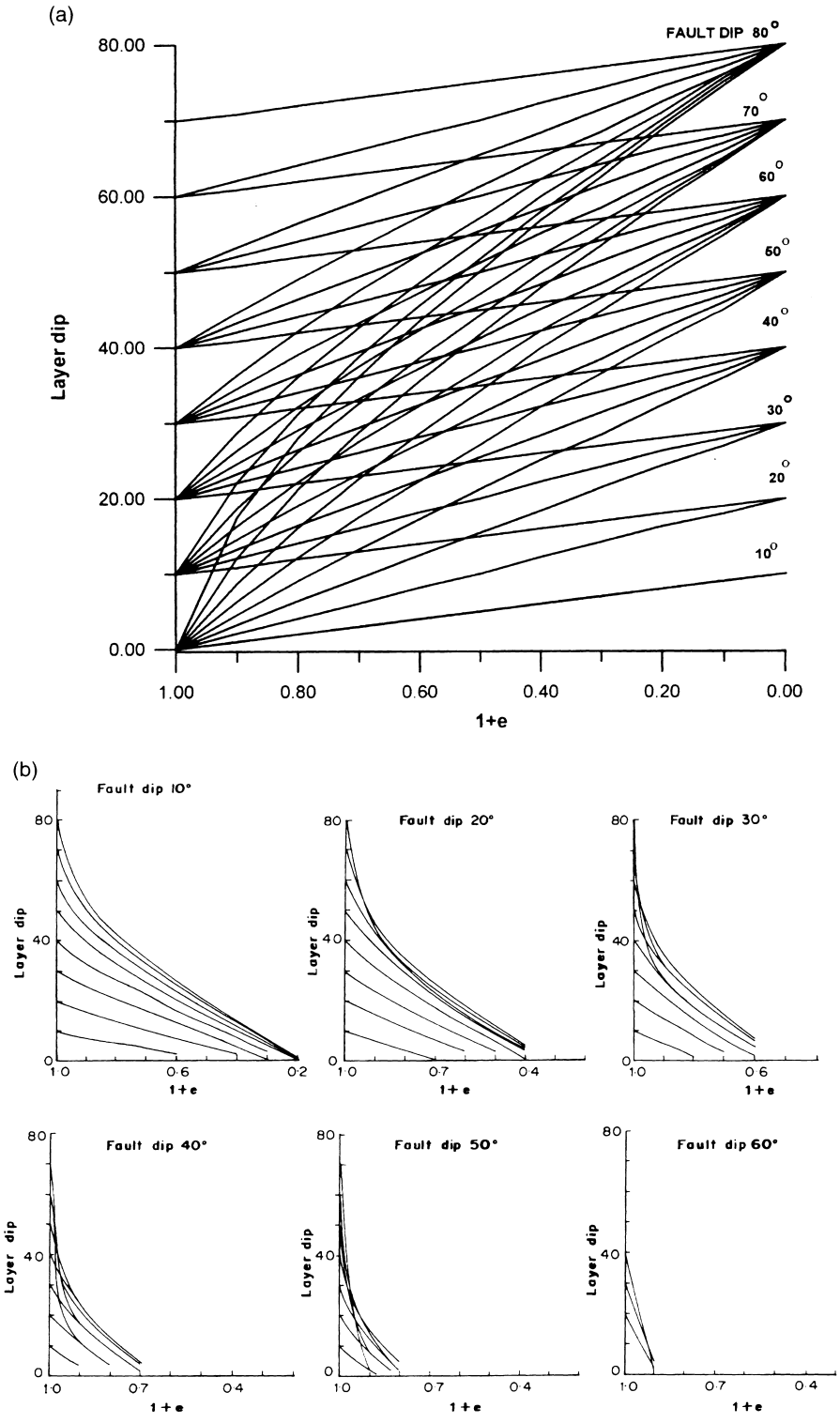

Fig. 2. (a) Relationships between shortening ($1 + e$) and layer dip, for different fault dips when fault and layer dip in the same direction. (b) Relationships between shortening ($1 + e$) and layer dip, for different fault dips when fault and layer dip in opposite directions.

tion was accompanied by a gradual clockwise rotation of the fold axial surfaces in harmony with the rotation of the hangingwall block along the listric fault. Thus, symmetric folds showed back-fold or hangingwall-vergent fold geometry (Fig. 4c). Fold development was not observed in the lower layers of the hangingwall, where the rotation amount of the layers along the fault was greater than predicted (Fig. 2a).

The development of multilayer hangingwall folds was coeval with large folds in the top and the bottom

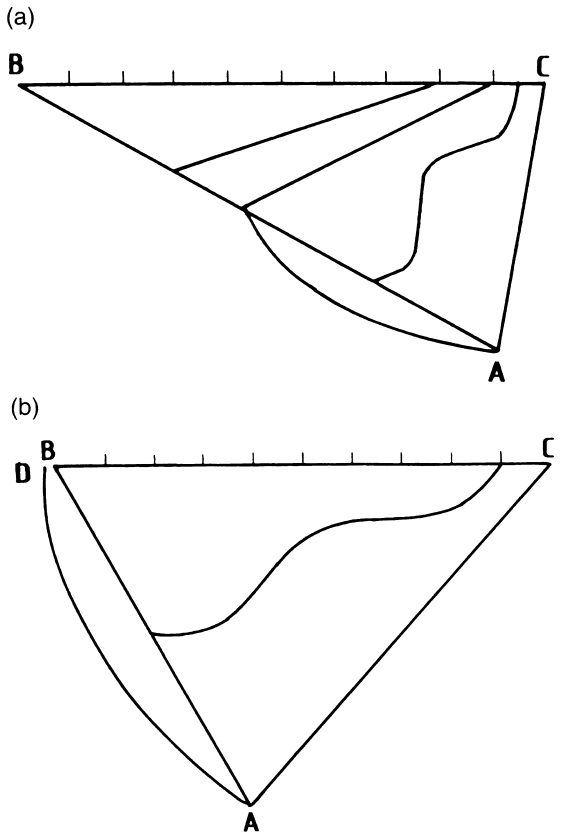

Fig. 3. Geometrical representation of changes in length of a layer (initial position AC) while rotation along a fault (AB) during pure shear deformation. (a) Fault dip 30°, layer dip 80°. (b) Fault dip 60°, layer dip 50°. The curve AD represents rotation of the line AC while maintaining a constant length during deformation.

matrix (Fig. 4c). A thrust fault conjugate to the main thrust initiated in the bottom matrix. It propagated into the footwall multilayers and produced a fault propagation fold. The fold quickly propagated upward in the footwall multilayer profile. The upper footwall layers folded in harmony with hangingwall layers because of layer parallelism and lack of displacement at the thrust tip. Lower footwall layers resemble the reverse fault drag whereas the upper layers resemble the normal fault drag thereby creating a dilation space (Δ, marked on Fig. 4d) in the region of reversal of layer dip. The decrease of fold interlimb angles, limb thinning and hinge thickening, development of limb thrust and fold locking were similar to multilayer folding in earlier experiments (Dubey, 1980; Behzadi and Dubey, 1980; Dubey and Behzadi, 1981).

The main listric thrust rotated gradually away from the axis of maximum compression (Dubey and Behzadi, 1981; Kusznir *et al.*, 1991; Coward, 1996). However, the central part of the thrust underwent a greater rotation (Fig. 4d). The displacement also varied along the thrust with a minimum displacement at the upper matrix–multilayer interface. The fault displa-

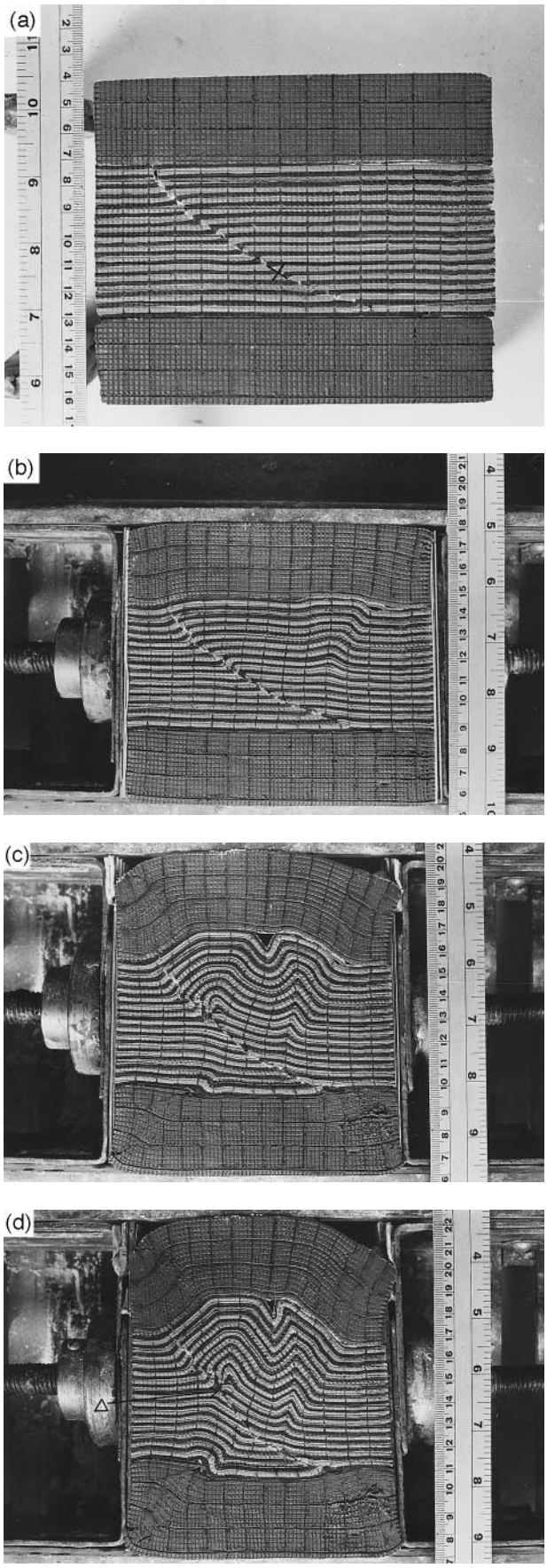

Fig. 4. Four stages in the deformation of a multilayer model showing development of folds near a listric fault. The total model shortening is (a) 0%, (b) 7%, (c) 17% and (d) 24%.

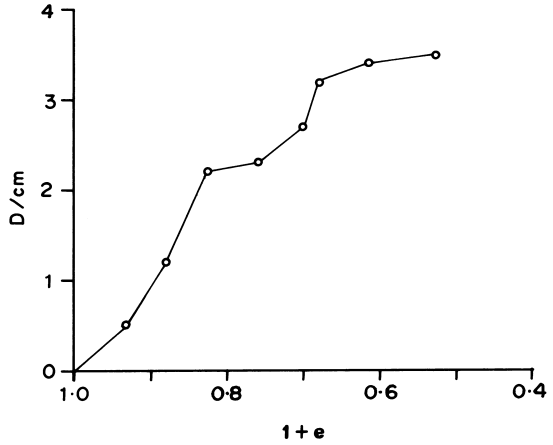

Fig. 5. Relationships between thrust displacement (D, in cm) and total model shortening ($1 + e$). The location for measurement of fault displacement (X) is shown on Fig. 4(a).

cement at point X (marked on Fig. 4a) increased up to 32% shortening (Fig. 5) and then decreased because of fault locking. This change was followed by extension of the model parallel to the strike of the thrust and the fold hinge lines (i.e. vertical axis of the press) (Dubey, 1980; Dubey and Bhat, 1986).

To understand the variation of buckle shortening and layer parallel strain across the multilayer profile, apparent layer strain (i.e. ratio of final length to original length determined by unfolding of the layer) was determined for different layers. A large ratio indicates a large layer parallel strain and a small ratio indicates a large buckle shortening. The relationship between total model strain ($1 + e$) and apparent layer strain (Fig. 6) indicates that a large buckle shortening in the hangingwall is characteristic of the 15th layer (from the bottom) and a large layer parallel shortening is characteristic of the third layer. Thus, the amount of

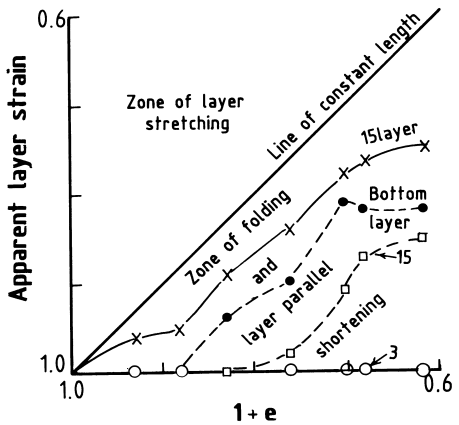

Fig. 6. Relationships between apparent layer strain and total model strain ($1 + e$) for different layers in the multilayer profile. Continuous lines: hangingwall layers; broken lines: footwall layers.

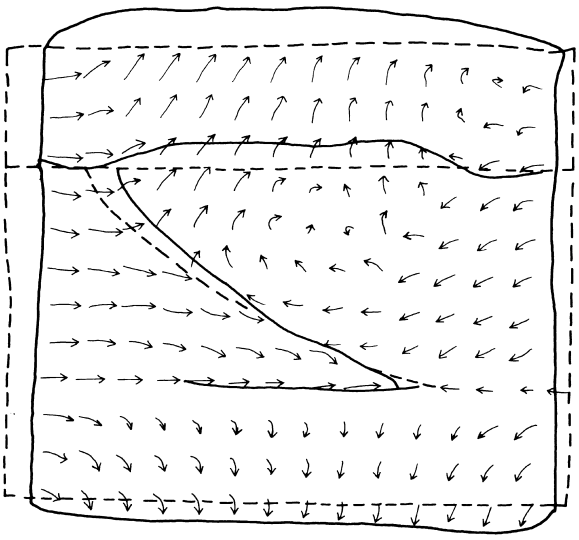

Fig. 7. The particle movement path field and rotation of the thrust in the experiment shown in Fig. 4. Broken lines represent initial outline of the model and the listric fault; continuous lines represent configuration of the model and the thrust after 12% shortening.

buckle shortening increased upwards in the profile. In contrast to the hangingwall layers, the footwall bottom layer showed a greater buckle shortening than the third hangingwall layer because of fold initiation in the bottom layer as fault propagation fold.

The particle movement path field was determined by tracing the intersection points of undeformed grid lines on a sheet, keeping the sheet on photographs of the successive stages of deformation and marking the new positions of the grid intersection points (Fig. 7, cf. Cobbold, 1975). In the lower part of the hangingwall, the movement paths are parallel to the thrust in its vicinity whereas a deflection away from the thrust was observed in the upper part, as a result of tilting of the hangingwall block. The tilt pattern was locally modified because of fold amplification in the hangingwall layers. The effect of displacement pattern on the folding of the top and bottom matrix is also evident in the diagram. The rotational pattern explains the increase in fault dip with an increase in deformation. The diagram also displays a point of zero displacement where the fold did not develop. In the footwall region, the movement paths were parallel to the axis of maximum shortening except close to the base of the thrust where the displacement pattern was modified by thrust related shear. Since the initial fault did not extend into the top and bottom matrix, the pattern in the footwall was that of a pure shear deformation (Ramsay and Huber, 1983, fig. 4.3D).

Experiment 2

In this experiment, the footwall layers were parallel to the axis of maximum shortening whereas the hang-

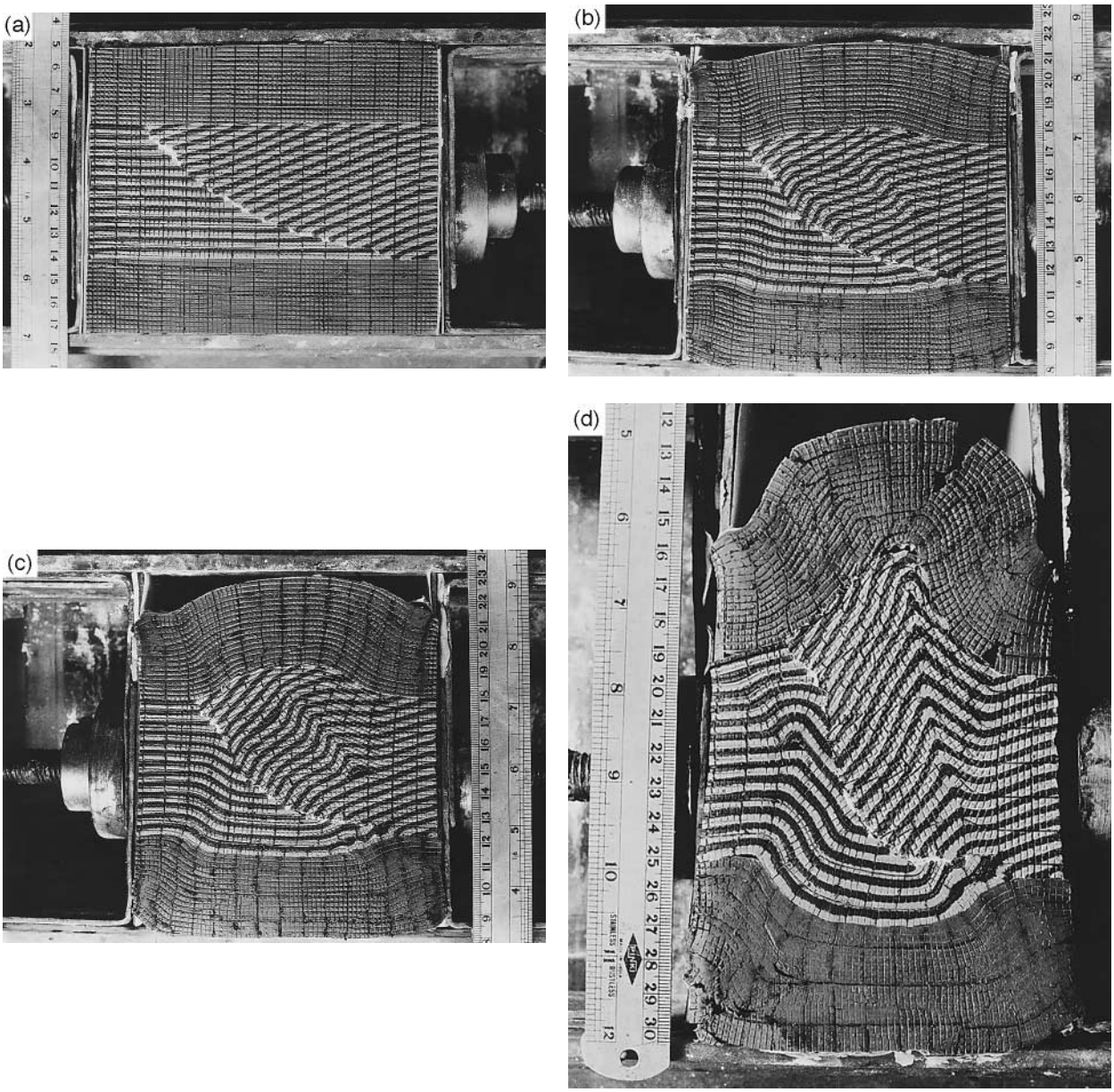

Fig. 8. Four stages in the deformation of a multilayer model. The total model shortening is (a) 0%, (b) 15%, (c) 20%, and (d) 36%.

ingwall layers had a dip opposite to the dip of the initial fault (Fig. 8a). This layer geometry could result during normal faulting of a rift phase, prior to positive inversion.

Two asymmetric anticlines with an intervening syncline were observed in the hangingwall at 15% shortening (Fig. 8b). The fold axial surfaces and the thrust dip are in the same direction. The fold near the thrust amplified up to 15% shortening and then the amplification rate dropped. A greater amplification was then observed in the second anticlinal fold at a distance from the thrust (Fig. 8c). The amplification decreased interlimb angles and straightened fold limbs, leading to unfolding of the near-thrust fold. The locking of the hangingwall folds was observed at 36% shortening (Fig. 8d). Fault displacement was insignificant hence the layers did not rotate along the thrust (cf. Fig. 4d).

The footwall folds initiated with a kink band geometry (Fig. 8b). Amplification of the hangingwall and footwall folds was accompanied by folding of the top and bottom matrix.

A relationship between total model strain $(1 + e)$ and apparent layer strain (for a single layer) (Fig. 9) reveals that the initial stages of deformation were marked by greater layer parallel shortening. The buckle folds initiated in the middle layers of the hangingwall (25th layer from the bottom) at 11% shortening and amplified up to 36% shortening. The 15th

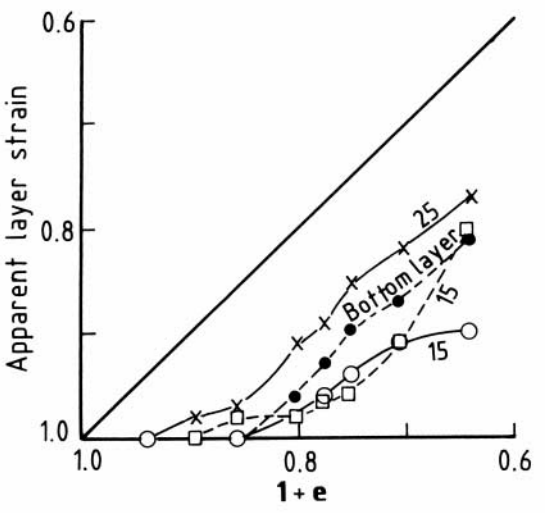

Fig. 9. Relationships between apparent layer strain and total model strain ($1 + e$) for four layers in the multilayer profile. Continuous lines: hangingwall layers; broken lines: footwall layers.

hangingwall layer from the bottom underwent an initial layer parallel shortening followed by folding at 15% shortening. The folds locked at 30% shortening. The initial layer parallel shortening was more prominent in the footwall layers, where folds initiated in different layers between 10 and 15% shortening. The buckle shortening was more prominent in the bottom layer soon after the initiation of folds whereas the 15th layer from the bottom showed a rapid increase in buckle shortening after 25% shortening. Limb thinning and hinge thickening were not observed.

Experiment 3

The model was constructed so that the footwall layers were parallel to the axis of maximum compression and the hangingwall layers had a dip of 20° in the dip direction of the initial fault (Fig. 10a). The orientation of the layers is expected in a compressional regime when thrusting precedes folding.

Asymmetric folds of two orientations were observed in the hangingwall at 10% shortening (Fig. 10b). The first one initiated at the thrust tip as a fault propagation fold. The initiation of the fold may be attributed to an early overlap of the thrust tip by the top layer as a result of layer parallel slip followed by thrusting. The second fold initiated in the lower hangingwall layers as a back fold (cf. Cobbold *et al.*, 1971; Mugnier *et al.*, 1994, fig. 5). The shear sense indicated by the asymmetric nature of the back fold was not in harmony with thrusting. At the lower levels along the thrust, a larger rotation of the layers and their parallel orientation with the thrust did not allow folding (Fig. 10c, cf. Fig. 2a). The hangingwall folds locked up at around 25% shortening. Additional shortening led to extension fractures across the layering and rotation of the axial surface in the thrust transport direction on a frontal ramp (Fig. 10d), as a result of the pure shear boundary conditions. The displacement at the thrust tip was small hence, the thrust did not penetrate the upper matrix.

Footwall folds initiated in the bottom layer (Fig. 10b) and became prominent at 29% shortening (Fig. 10c). The asymmetric footwall folds indicated a shear sense in conformity with the thrusting. The footwall folds were coeval with the large buckle folds developed in the bounding medium.

A SUMMARY OF THE EXPERIMENTAL RESULTS

At the onset of deformation, fold initiation and amplification were prominent in the hangingwall, irrespective of the initial orientation of the layering. However, when the initial layering (both in the hangingwall and the footwall) was parallel to the axis of maximum compression, the initiation of folds took place at an early stage of deformation. The progressive deformation resulted in a decrease in fold interlimb angles and an increase in fault dip. A continuous change of interlimb angles and fault dip made it impossible to establish a systematic relationship between the ramp angle and the interlimb angles (cf. Jamison, 1987).

The rate of thrust displacement and total displacement varied with variation in orientation of layers and thrust dip. Maximum displacement occurred when hangingwall layers and the thrust dipped in the same direction and the displacement direction was subparallel to layering. Minimum displacement occurred when the thrust and layers dipped in opposite directions. In all the experiments, maximum displacement occurred in the central part of the thrust, gradually decreasing towards the tip. This result contrasts with experiments by McClay and Scott (1991) where a mylar sheet on the upper surface of the rigid footwall was attached to the moving wall and the displacement along the ramp–flat fault was made proportional to the displacement along the moving wall.

The pattern of the particle movement path field resulted from a combination of; (i) pure shear deformation of the model, (ii) displacement along the thrust, (iii) rotation of hangingwall along the listric fault, and (iv) folding of the multilayers (cf. Couples *et al.*, 1994, fig. 11). Hence, the displacement paths were not always parallel to the thrust but at an angle to it.

GEOLOGICAL IMPLICATIONS OF THE RESULTS

When frictional effects are insignificant along a thrust surface (as discussed in the geometrical model) rotation of the hangingwall layers plays an important

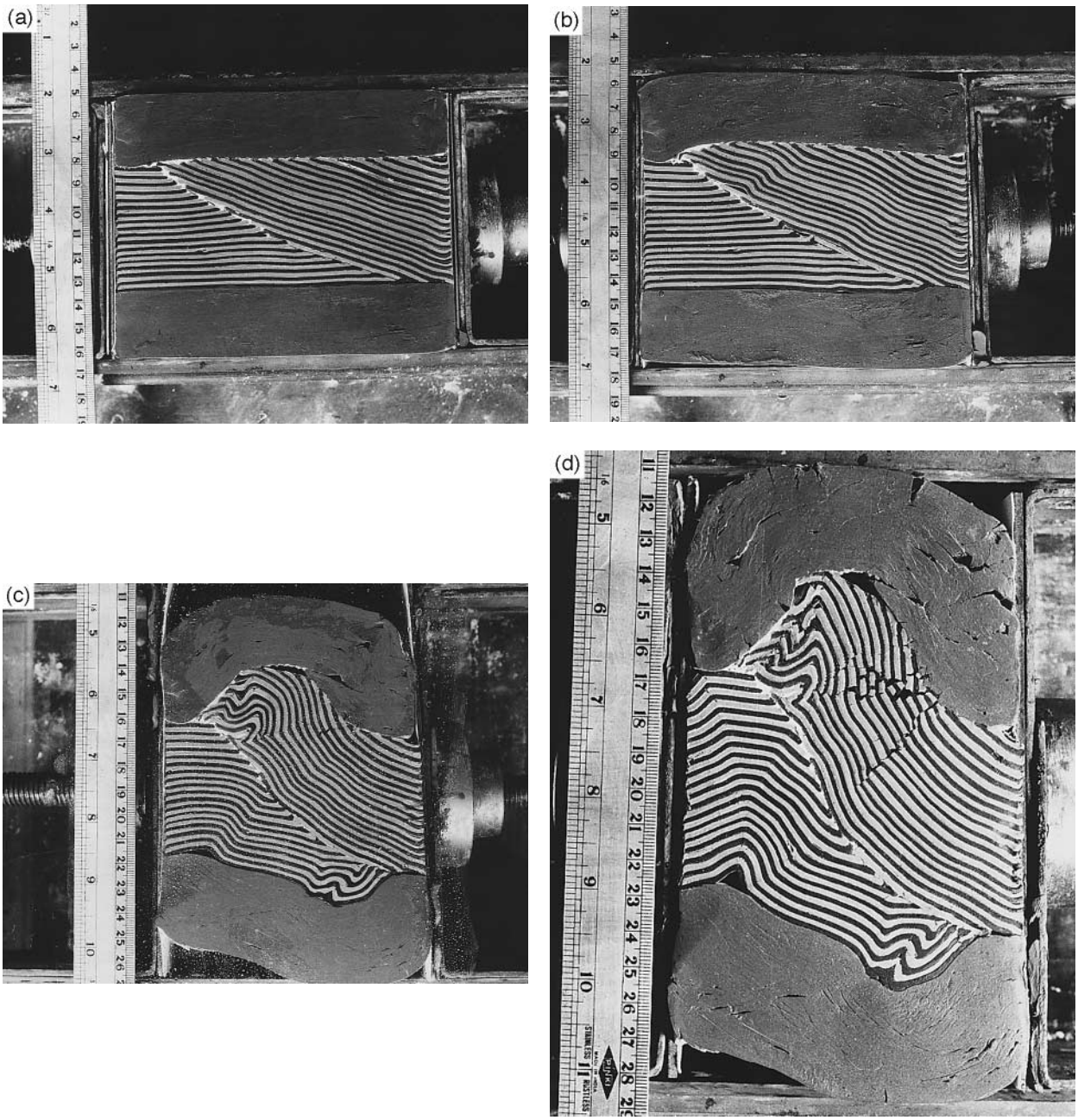

Fig. 10. Four stages in the deformation of a multilayer model. The total model shortening is (a) 0%, (b) 10%, (c) 29%, and (d) 38%.

role in deformation. The rotation may bring the layers into zone 1 of the strain ellipse (Ramsay, 1967, fig. 3.62) where progressive shortening leads to stretching of the layers thereby inhibiting the initiation of folds in the vicinity of the thrust. The resulting structure in the hangingwall will be that of a reverse drag (Fig. 11a) (cf. Hamblin, 1965). Friction along the fault is likely to produce normal drag (Fig. 11b).

The amount of layer rotation along a well lubricated fault is proportional to the dip of the thrust hence a higher dip results in a larger rotation (Fig. 2). This implies that the positive listric faults (i.e. listric faults with a decrease of dip with depth) are expected to show a decrease in layer rotation with an increase in depth. The variation of layer rotation may result in the formation of a number of dilation spaces along the thrust (Fig. 12). The dilation initiates at regions of variation in thrust dip and the area of each dilation depends on the amount of dip change, frictional effects along the thrust surface, and dip of the hangingwall layers (Fig. 2). The dilation spaces may also form at an angular unconformity (Fig. 13). The dilation spaces so formed may serve as sites for secondary mineral deposits or as oil traps. In a brittle–ductile regime,

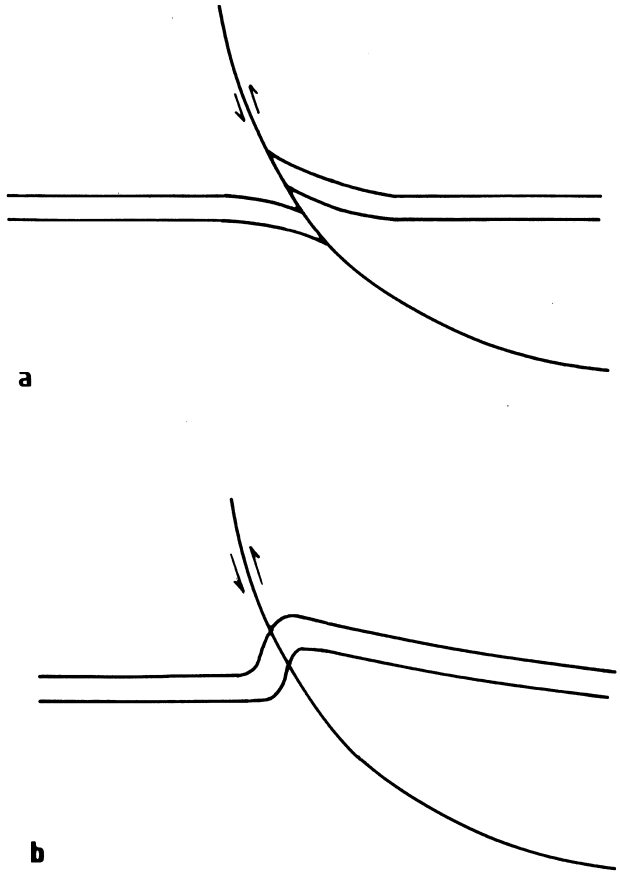

Fig. 11. Displacement of layer along a thrust and formation of (a) reverse drag, and (b) normal drag.

folds with the described geometries may form above and below the unconformity (Fig. 13c).

A variation of layer rotation and different fold geometries may also result within a stratigraphic sequence with variation in fault geometry. For example, Fig. 14(a) depicts a pre- to post-rift sequence. A later compressional phase results in reactivation of the earlier normal fault as thrust. The layer with a dip opposite to the dip direction of the thrust (layer A) undergoes a larger rotation as compared to the horizontal layer (layer C), along a fault of uniform dip (see Fig. 2). The larger rotation of layer (A) in the profile accompanied by resistance to displacement of layer C from above, may result in the formation of an asymmetric fold in the overlying layer (C) near the thrust

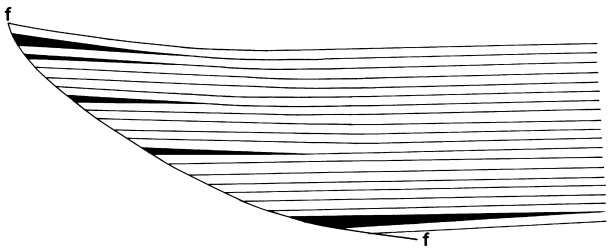

Fig. 12. Formation of dilation spaces (marked black) as a result of variation of layer rotation along a listric fault (ff).

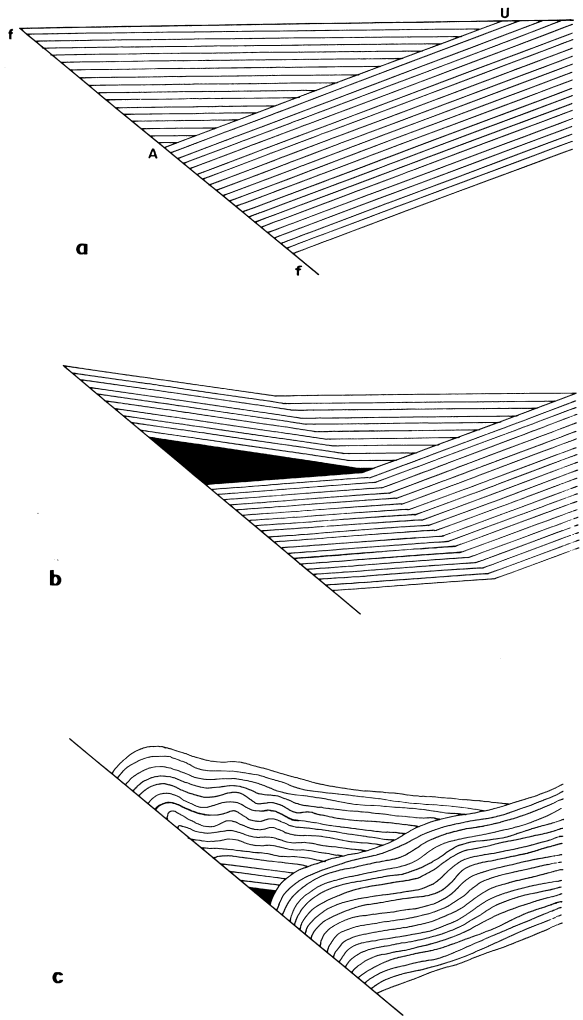

Fig. 13. (a) Initial configuration of layers, an angular unconformity (AU), and a fault (ff). (b). Variation in the rotation of layers as a result of variation in the initial dip of the layers and formation of dilation space (marked black), in a brittle regime. (c) Development of different fold geometries in older and younger sequence of rocks and formation of dilation space, in a brittle–ductile regime.

(Fig. 14b) (cf. Berger and Johnson, 1980; Gillcrist *et al.*, 1987, figs 27 and 28). A decrease of thrust dip with depth is not an essential condition for the described model (cf. Letouzey, 1990, fig. 13). If the fault geometry is characterized by a ramp–flat structure (Fig. 14c), the rotation of the horizontal layer is further reduced on a low dip segment of the fault (see Fig. 2) thereby resulting in a ramp anticline.

CONCLUSIONS

Displacement along a thrust leads to tilting and rotation of hangingwall layers. The rotation magnitude depends on the initial layer orientation and thrust dip. A variation of thrust dip with depth (e.g. listric thrust fault) may result in variation of layer rotation thereby forming a number of dilation spaces near the thrust.

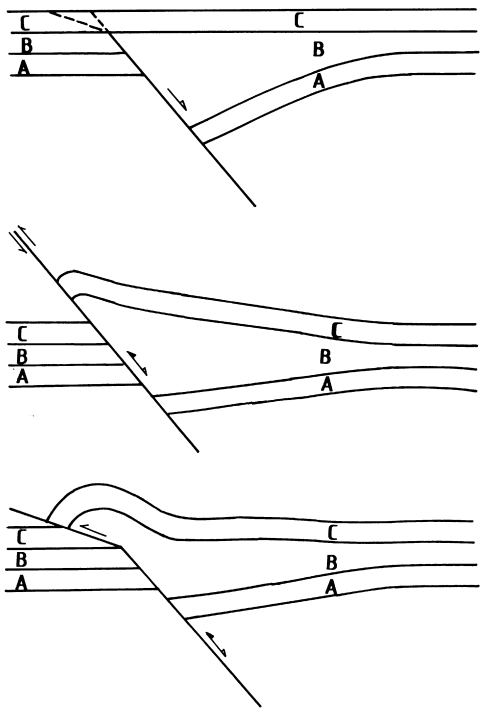

Fig. 14. Effect of fault geometry on the development of folds. (a). Initial configuration of the stratigraphic sequence. A, pre-rift; B, syn-rift; C, post-rift sequence. (b) Formation of an asymmetric fold at a uniformly dipping thrust. (c) Formation of a ramp anticline over a ramp–flat profile.

Location of the dilation spaces, which may act as potential sites for secondary mineral deposits, can be predicted with the knowledge of thrust geometry and orientation of the hangingwall layers.

Contractional and extensional structures may develop simultaneously at upper and lower levels, respectively, in a multilayer sequence of uniform initial orientation but with variation of listric thrust dip. A larger rotation of underlying layer and resistance to displacement from above may trigger off folding in the hangingwall layers near the thrust. Geometry and orientation of hangingwall folds, coeval with thrusting, are characteristic of the initial layer orientation. Hence, the study of hangingwall folds can lead to understanding of the initial layer orientation and tectonic history of a rifted basin.

Viewing the results in the Himalayan context, the sharp anticlines in the Sub-Himalayan sedimentary sequences of rocks (Gansser, 1964) have been described and simulated as fault propagation folds (Dubey and Bhat, 1986) located above blind thrusts (Yeats and Lillie, 1991). Since the area is seismically active, a knowledge of thrust displacement and rotation of subsurface layers will help in understanding the future seismic activity in the region.

Acknowledgements—Several discussions were made with V. C. Thakur, N. K. Saini and M. I. Bhat. The manuscript was greatly improved by the review comments of Dr Dave Waltham. A research grant from the Department of Science and Technology, Government of India, is gratefully acknowledged.

REFERENCES

Behzadi, H. and Dubey, A. K. (1980) Variation of interlayer slip in space and time during flexural folding. *Journal of Structural Geology* **2,** 453–457.

Berger, P. and Johnson, A. M. (1980) First order analysis of deformation of a thrust sheet moving over a ramp. *Tectonophysics* **70,** T9–T24.

Buchanan, P. G. and McClay, K. R. (1991) Sandbox experiments of inverted listric and planar fault systems. *Tectonophysics* **188,** 97–115.

Cobbold, P. R. (1975) Fold propagation in single embedded layers. *Tectonophysics* **27,** 333–351.

Cobbold, P. R., Cosgrove, J. W. and Summers, J. M. (1971) Development of internal structures in deformed anisotropic rocks. *Tectonophysics* **12,** 23–53.

Cooper, M. A. and Williams, G. D. (1989) Inversion Tectonics. *Geological Society Special Publication* **44,** 375.

Couples, G. D., Stearns, D. W. and Handin, J. W. (1994) Kinematics of experimental forced folds and their relevance to cross-section balancing. *Tectonophysics* **233,** 193–213.

Coward, M. P. (1996) Balancing sections through inverted basins. In *Modern Developments in Structural Interpretation, Validation and Modelling*, eds P. G. Buchanan and D. A. Nieuwland, pp. 51–77. Geological Society Special Publication, **99**.

Dubey, A. K. (1980) Late stages in the development of folds as deduced from model experiments. *Tectonophysics* **65,** 311–322.

Dubey, A. K. and Cobbold, P. R. (1977) Noncylindrical flexural slip folds in nature and experiment. *Tectonophysics* **38,** 223–239.

Dubey, A. K. and Behzadi, H. (1981) Development of flexural slip folds, overlapping boudins and extension faults in multilayered materials: field evidence and experimental model. *Bulletin Geological Society of India* **22,** 274–284.

Dubey, A. K. and Bhat, M. I. (1986) The role of reactivation of pre-rift basement listric faults in the structural evolution of the Himalaya: an experimental study. In *Himalayan Thrusts and Associated Rocks*, ed. P. S. Saklani, pp. 265–290. Current Trends in Geology, **9**.

Gansser, A. (1964) *Geology of the Himalayas*. Interscience, London.

Gillcrist, R., Coward, M. P. and Mugnier, J.-L. (1987) Structural inversion and its controls: examples from the Alpine foreland and the French Alps. *Geodinamica Acta* **1,** 5–34.

Hamblin, W. K. (1965) Origin of "reverse drag" on the downthrown side of normal faults. *Geological Society of America Bulletin* **76,** 1145–1164.

Huiqi, L., McClay, K. R. and Powell, D. (1992) Physical models of thrust wedges. In *Thrust Tectonics*, ed. K. R. McClay, pp. 71–81. Chapman & Hall, London.

Jamison, W. R. (1987) Geometric analysis of fold development in overthrust terranes. *Journal of Structural Geology* **9,** 207–219.

Kusznir, N. J., Marsden, G. and Egan, S. S. (1991) A flexural-cantilever simple-shear/pure-shear model of continental lithosphere extension: applications to the Jeanne d'Arc Basin, Grand Banks and Viking Graben, North Sea. In *The Geometry of Normal Faults*, eds A. M. Roberts, G. Yielding and B. Freeman, pp. 41–60. Geological Society Special Publication, **56**.

Letouzey, J. (1990) Fault reactivation, inversion and fold thrust belt. In *Petroleum and Tectonics in Mobile Belts*, ed. J. Letouzey, pp. 101–128. Editions Technip.

McClay, K. R. (1989) Analogue models of inversion tectonics. In *Inversion Tectonics*, eds M. A. Cooper and G. D. Williams, pp. 41–59. Geological Society Special Publication, **44**.

McClay, K. R. and Ellis, P. G. (1987) Analogue models of extensional fault geometries. In *Continental Extensional Tectonics*, eds M. P. Coward, J. F. Dewey and P. L. Hancock, pp. 109–125. Geological Society Special Publication, **28**.

McClay, K. R. and Scott, A. D. (1991) Experimental models of hangingwall deformation in ramp–flat listric extensional fault systems. *Tectonophysics* **188,** 85–96.

McClay, K. R. and Buchanan, P. G. (1992) Thrust faults in inverted extensional basins. In *Thrust Tectonics*, ed. K. R. McClay, pp. 93–104. Chapman & Hall, London.

Mugnier, J. L., Mascle, G. and Faucher, T. (1994) The structures of the frontal thrust belt of Himalaya (Siwaliks of western Nepal). *Himalayan Geology* **15,** 245–261.

Ramsay, J. G. (1967) *Folding and Fracturing of Rocks*. McGraw Hill, New York.

Ramsay, J. G. (1974) Development of chevron folds. *Bulletin Geological Society of America* **85,** 1741–1754.

Ramsay, J. G. and Huber, M. I. (1983) *The Techniques of Modern Structural Geology, Volume 1, Strain Analysis*. Academic Press, London.

Ramsay, J. G. and Huber, M. I. (1987) *The Techniques of Modern Structural Geology, Volume 2, Folds and Fractures*. Academic Press, London.

Suppe, J. (1983) Geometry and kinematics of fault bend folding. *American Journal of Science* **283,** 684–721.

Williams, G. D., Powell, C. M. and Cooper, M. A. (1989) Geometry and kinematics of inversion tectonics. In *Inversion Tectonics*, eds M. A. Cooper and G. D. Williams, pp. 3–15. Geological Society Special Publication, **44**.

Yeats, R. S. and Lillie, R. J. (1991) Contemporary tectonics of the Himalayan frontal fault system: folds, blind thrusts and the 1905 Kangra earthquake. *Journal of Structural Geology* **13,** 215–225.